INTERNATIONAL JOURNAL FOR NUMERICAL METHODS IN FLUIDS
Int. J. Numer. Meth. Fluids 2009; **61**:1–22
Published online 23 October 2008 in Wiley InterScience (www.interscience.wiley.com). DOI: 10.1002/fld.1941

Edge-based finite element implementation of the residual-based variational multiscale method

Erb F. Lins[1,‡], Renato N. Elias[1], Gabriel M. Guerra[2], Fernando A. Rochinha[2] and Alvaro L. G. A. Coutinho[1,*,†]

[1]*Center for Parallel Computing and Department of Civil Engineering, COPPE/Federal University of Rio de Janeiro, PO Box 68506, Rio de Janeiro, RJ 21945, Brazil*
[2]*Department of Mechanical Engineering, COPPE/Federal University of Rio de Janeiro, PO Box 68503, Rio de Janeiro, RJ 21945, Brazil*

SUMMARY

In this work we extend our edge-based stabilized finite element incompressible flow solver to turbulence modeling with the residual-based variational multiscale (RB-VMS) method. Using the advective-form of the convection term of the Navier–Stokes equations, RB-VMS is implemented as a straightforward extension of standard stabilized methods with a modified advective velocity. This requires minimum modification of the existing highly optimized code. Two test cases were solved to assess accuracy and performance of the present implementation. First, the laminar incompressible flow past a circular cylinder at $Re = 100$ and second, the fully turbulent incompressible flow in a lid-driven cubic cavity at $Re = 12\,000$. Comparisons were made with standard stabilized finite element formulations, highly resolved numerical simulations and experimental data. Results have shown that the present implementation is able to achieve reasonable accuracy without performance degradation in different flow regimes. Copyright © 2008 John Wiley & Sons, Ltd.

Received 11 March 2008; Revised 30 August 2008; Accepted 2 September 2008

KEY WORDS: variational multiscale method; turbulence; edge-based computations; stabilized finite elements; parallel computing; large eddy simulation

1. INTRODUCTION

Flow of incompressible fluids is often in turbulent state. The incompressible Navier–Stokes equations represent the mathematical model for both laminar and turbulent flow states. Solving for all

*Correspondence to: Alvaro L. G. A. Coutinho, Center for Parallel Computing and Department of Civil Engineering, COPPE/Federal University of Rio de Janeiro, PO Box 68506, Rio de Janeiro, RJ 21945, Brazil.
†E-mail: alvaro@nacad.ufrj.br
‡Present address: Department of Mechanical Engineering, Federal University of Para, Belem, PA 66075-900, Brazil.

Contract/grant sponsor: PETROBRAS Research Center
Contract/grant sponsor: MCT/CNPq

the length and temporal scales present in turbulent flows, a process known as direct numerical simulation (DNS), is still a challenge, particularly at high Reynolds numbers. A viable alternative is large eddy simulation (LES), where only the large flow structures are solved, while the effects of smaller structures on the large ones are modeled [1]. The variational multiscale method (VMS) [2, 3] provides a theoretical framework for general multiscale problems in computational mechanics by separating the scales of interest in a predetermined number of groups (usually two, coarse and fine scales). Inspired by traditional LES, VMS was initially applied to turbulent flows by generating eddy viscosities (static and dynamic) associated only with the fine scales. This approach has been applied successfully to a number of problems, with several discretization methods. Please see Hughes *et al*. [4], Calo [5] and Gravemeier [6] for detailed reviews.

VMS is also closely linked to stabilized methods, particularly for solving the incompressible Navier–Stokes equations [4]. Stabilization is needed to prevent spurious oscillations in convection-dominated flows when under-resolved meshes are employed. It is also needed to prevent undesired pressure oscillations when equal-order interpolations for velocity and pressure are used. In turbulent flow, small-scales physics become crucial and the beneficial effects of stabilization may be used to generate numerically eddy viscosities needed in LES [7–10]. Practical examples of such an approach, in fluid–structure interaction, dispersion of radionuclides in nuclear power plants and density currents may be found in [11–13]. In these, different numerical implementations are present (space–time, semi-discrete, fully coupled, segregated) and additional computational devices, such as mesh adaptation or discontinuity-capturing is often employed. For the orthogonal subgrid scale stabilized finite element method, Guasch and Codina [14] proved that the contribution to the energy balance equations of the stabilized terms is proportional to the physical dissipation rate. Nevertheless, according to Bazilevs *et al*. [15], traditional eddy viscosities are inefficient in representing fine-scales dissipation mechanisms and introduce inconsistencies.

As a remedy, the residual-based variational multiscale (RB-VMS) is emerging as a new concept in LES. It was introduced in Calo [5], who studied bypass transition on a zero-pressure gradient flat plate. Calo has also shown an implementation of RB-VMS on a second-order finite volume code and described how to derive a weak formulation that yields an equivalent discrete equation system. Gravemeier *et al*. [16] studied turbulent flows in a channel at $Re = 180$ with an RB-VMS finite element method showing the importance of higher-order polynomial approximations. Bazilevs *et al*. [15] presented an LES-type VMS theory of turbulence and tested it on forced homogeneous turbulence, isotropic turbulence and turbulent homogeneous channel flows, stressing the superior quality of NURBS elements with respect to classical finite elements. Akkerman *et al*. [17] examined the role of continuity in computation of turbulent flows with RB-VMS applied to the advective-form of the governing equations.

Edge-based data structures have been introduced in the finite element context to speed up explicit compressible flow simulations [18]. More recently edge-based implementations have been introduced for several other problems. Ribeiro *et al*. [19] presented an edge-based implementation for stabilized semi-discrete and space–time finite element formulations for shallow water equations, Catabriga and Coutinho [20] for the implicit Streamline-Upwind Petrov–Galerkin (SUPG) solution of the Euler equations, Soto *et al*. [21] for incompressible flow problems with fractional step methods, Kraft *et al*. [22] for a segregated symmetric stabilized solution of incompressible flow with heat transfer. Parallel simulations of viscoplastic, free-surface flows and density currents employing stabilized edge-based formulations may be found in [13, 23, 24]. Ribeiro and Coutinho [25] show that for unstructured grids composed by tetrahedra, edge-based data structures decrease the number of floating point operations and indirect addressing in matrix–vector products needed

DOI: 10.1002/fld

in Krylov space solvers and diminish the storage area to hold Jacobians compared with element and pointwise data structures, particularly for problems involving many degrees of freedom. The construction of edge operations is completely algebraic [13, 20, 22–25], based on the concept of disassembling element operators, regardless of the particular underlying finite element formulation.

In this work, we extend our edge-based stabilized finite element incompressible flow solver to turbulence with RB-VMS. The main characteristics of our basic solver are: SUPG [26], pressure-stabilizing/Petrov–Galerkin (PSPG) and least-squares incompressibility constraint (LSIC) stabilized finite element formulation, [27, 28]; implicit time marching scheme with adaptive time stepping control; advanced inexact Newton solvers; edge-based data structures to save memory and improve performance; support to message passing and shared memory parallel programming models; LES by Smagorinsky's model and volume-of-fluid (VOF) extensions to track the evolving free surfaces [23]. In the following section we derive the RB-VMS formulation, and in the sequence we show how to incorporate it, using the advective-form of the convection term of the Navier–Stokes equations [17], as a straightforward extension of standard stabilized methods with a modified advective velocity. This requires minimum modification of the existing highly optimized code. Two test cases were solved in Section 4, a laminar and a turbulent problem. We solved the incompressible flow past a circular cylinder at $Re=100$ and compared RB-VMS with standard stabilized formulations. We have shown that RB-VMS presented similar accuracy and performance as SUPG/PSPG/LSIC in this laminar test case. Then, we compare our results in the lid-driven cubic cavity at $Re=12\,000$ problem, where recent LES, DNS and experimental results are available [29]. We noted that the present implementation was able to capture most of the relevant turbulent flow features with reasonable accuracy when compared with highly resolved numerical simulations and experimental data. The paper ends with a summary of our main conclusions.

2. THE INCOMPRESSIBLE NAVIER–STOKES EQUATIONS AND MULTISCALE TURBULENCE MODELING

Unlike many other multi-scale phenomena, turbulence is believed to be accurately described by using one unique equation through all present scales. Indeed, geometrical patterns with the shape of eddies are replicated in different spatial scales and the incompressible Navier–Stokes equations are often adopted for modeling turbulent flows.

The Navier–Stokes equations lead to the following nonlinear mathematical problem to be solved: Let $\Omega\subset\mathbb{R}^3$ be an open bounded region, where flow occurs, with a piecewise regular boundary Γ. Find the pressure p (divided by the constant density) and the velocity $\mathbf{u}$ fields satisfying the following equations along the time interval $[0,t_f]$:

$$\frac{\partial\mathbf{u}}{\partial t}+\mathbf{u}\cdot\nabla\mathbf{u}-\nabla\cdot\boldsymbol{\sigma}=\mathbf{f}\quad\text{on }\Omega\times[0,t_f] \tag{1}$$

$$\nabla\cdot\mathbf{u}=0\quad\text{on }\Omega\times[0,t_f] \tag{2}$$

with $\mathbf{f}$ the body force vector per unity density and $\boldsymbol{\sigma}$ the stress tensor given as

$$\boldsymbol{\sigma}(p,\mathbf{u})=-p\mathbf{I}+\mathbf{T} \tag{3}$$

where $\mathbf{I}$ is the identity tensor and $\mathbf{T}$ is the deviatoric stress tensor,

$$\mathbf{T}=2\nu\boldsymbol{\varepsilon}(\mathbf{u}) \tag{4}$$

DOI: 10.1002/fld

In Equation (4) ν is the kinematic viscosity and $\boldsymbol{\varepsilon}(\mathbf{u})$ is the strain rate tensor defined as

$$\boldsymbol{\varepsilon}(\mathbf{u}) = \tfrac{1}{2}(\nabla\mathbf{u} + (\nabla\mathbf{u})^{\mathrm{T}}) \tag{5}$$

Essential and natural boundary conditions for Equation (1) are $\mathbf{u} = \mathbf{g}$ on Γ_g and $\mathbf{n}\cdot\boldsymbol{\sigma} = \mathbf{h}$ on Γ_h, where Γ_g and Γ_h are complementary subsets of the domain boundary Γ. Functions $\mathbf{g}$ and $\mathbf{h}$ are given and $\mathbf{n}$ is the unit outward normal vector of Γ. A divergence-free velocity field $\mathbf{u}_0$ is the initial condition. Moreover, for many applications, we are interested in the domains and boundaries that change along time and are not completely known in advance. Typically, we are referring to free surfaces flows, in which a part of the boundary should be tracked along the flow [13, 23].

The above mathematical problem, represented by the balance of momentum, continuity equation, initial and boundary conditions, is recast into a weak formulation described by: Find the pair $(\mathbf{u}, p) \in V^* = V \times P, \forall(\mathbf{w}, q) \in W^* = W \times Q$, such that:

$$\left(\frac{\partial\mathbf{u}}{\partial t}, \mathbf{w}\right)_\Omega + (\mathbf{u}\cdot\nabla\mathbf{u}, \mathbf{w})_\Omega + (\boldsymbol{\sigma}(p, \mathbf{u}), \boldsymbol{\varepsilon}(\mathbf{w}))_\Omega + (\nabla\cdot\mathbf{u}, q)_\Omega = (\mathbf{f}, \mathbf{w})_\Omega + (\mathbf{h}, \mathbf{w})_{\Gamma_h} \tag{6}$$

where $(.,.)_\Omega = \int_\Omega (\cdot,\cdot)\,\mathrm{d}\Omega$ is the standard scalar product in $L^2(\Omega)$, the space of functions that are square integrable, and the trial spaces are defined as

$$V = \{\mathbf{u}(.,t) | \mathbf{u}(.,t) \in H^1(\Omega)^3; \mathbf{u} = \mathbf{g} \text{ on } \Gamma_g\} \tag{7}$$

$$P = \left\{ p(.,t) | p(.,t) \in L^2(\Omega); \int_\Omega p\,\mathrm{d}\Omega = 0 \right\} \tag{8}$$

with W^* being the corresponding weight space.

At this point, it is worth mentioning that the above weak formulation provides the basis for a Galerkin finite element approximation, which can present an unstable behavior. Spurious oscillations in the Galerkin formulation can appear due to incompatible spaces (continuous or discrete) and/or dominant advection. Both drawbacks can be handled by the use of stabilization [26–28], in which residual terms weighted by tuned parameters are appended to the above weak formulation. In the following, VMS is introduced in order to develop formulations that, at the same time, handle possible instabilities and provide a convenient theoretical framework for incorporating turbulence modeling in the LES sense.

Lately, VMS has been recognized as a new paradigm for building stabilized finite element formulations, in which extra stability stems from encoding the dynamics of the fine scales [15, 17]. In that sense, the first step consists of the multiscale decomposition of the original fields,

$$\mathbf{u} = \mathbf{u}^h + \mathbf{u}' \tag{9}$$

$$p = p^h + p' \tag{10}$$

where $(\mathbf{u}^h, p^h)$ and $(\mathbf{u}', p')$ stand for the coarse and fine scale components of the solution, respectively. Indeed, what one has in mind is an *a priori* decomposition of V^* into a direct sum of spaces, that is, $V^h \oplus V'$. The coarse scale is directly associated with a finite element approximation of the problem to be performed over the partition of the domain into non-overlapping elements Ω^e with characteristic length h.

It is important to mention that different formulations departing from the above *ab initio* decomposition, based on finite element approximations or not, have been introduced recently [4, 6]. They

DOI: 10.1002/fld

mainly differ in the way the fine-scale solution $\mathbf{u}'$ is addressed and how it is approximated. Here, we reproduce the main steps toward the formulation proposed in [15, 17]. This formulation can be understood as a new LES modeling paradigm not relying on spatial filters or eddy viscosities as they can pose severe theoretical restrictions related to the commutation between spatial and time derivatives or when complex domains are to be considered.

The decompositions (9) and (10) are plugged into Equation (6) and the linearity on the second slot is explored such that the following equations are obtained:

$$\left(\frac{\partial(\mathbf{u}^h+\mathbf{u}')}{\partial t},\mathbf{w}^h\right)_\Omega+((\mathbf{u}^h+\mathbf{u}')\cdot\nabla(\mathbf{u}^h+\mathbf{u}'),\mathbf{w}^h)_\Omega+(\boldsymbol{\sigma}(p^h+p',\mathbf{u}^h+\mathbf{u}'),\boldsymbol{\varepsilon}(\mathbf{w}^h))_\Omega$$
$$+(\nabla\cdot(\mathbf{u}^h+\mathbf{u}'),q^h)_\Omega=(\mathbf{f},\mathbf{w}^h)_\Omega+(\mathbf{h},\mathbf{w}^h)_{\Gamma_h}\quad\forall(\mathbf{w}^h,q^h)\in W^h\times P^h \tag{11}$$

$$\left(\frac{\partial(\mathbf{u}^h+\mathbf{u}')}{\partial t},\mathbf{w}'\right)_\Omega+((\mathbf{u}^h+\mathbf{u}')\cdot\nabla(\mathbf{u}^h+\mathbf{u}'),\mathbf{w}')_\Omega+(\boldsymbol{\sigma}(p^h+p',\mathbf{u}^h+\mathbf{u}'),\boldsymbol{\varepsilon}(\mathbf{w}'))_\Omega$$
$$+(\nabla\cdot(\mathbf{u}^h+\mathbf{u}'),q')_\Omega=(\mathbf{f},\mathbf{w}')_\Omega+(\mathbf{h},\mathbf{w}')_{\Gamma_h}\quad\forall(\mathbf{w}',q')\in W'\times P' \tag{12}$$

Rearranging the terms in Equation (12) and applying integration by parts, the equation corresponding to the fine scales is now cast as

$$(L_u(\mathbf{u}',p'),\mathbf{w}')_{\Omega^e}=(\mathbf{r}_\mathrm{M}(\mathbf{u}^h,p^h),\mathbf{w}')_{\Omega^e}\quad\forall\mathbf{w}'\in V'(\Omega_e) \tag{13}$$

where L_u is a compact notation for the advective–diffusive operator having as advective velocity $\mathbf{u}=\mathbf{u}^h+\mathbf{u}'$ and $\mathbf{r}_\mathrm{M}$ is the residual associated with the momentum equation. Note also that q' has been made zero.

Equation (13) might be interpreted as the one governing the response of the fine scales driven by the residual of the coarse-scale equation, $\mathbf{r}_\mathrm{M}$. The development of this equation has assumed that:

(i) The velocity fine-scales component vanishes on the element boundaries, which implies that terms involving integrals over inter-element interfaces are also zero. This introduces an approximation for $\mathbf{u}'$ inspired on the so-called bubble functions.
(ii) The time dependence of $\mathbf{u}'$ is not considered, leading to a quasi-static modeling of the fine scales. The effects of taking into account the time dependence of $\mathbf{u}'$ are investigated in [30].

Despite the above simplifying hypotheses, $\mathbf{u}'$ is defined in an infinite-dimensional space and here it will not be solved but approximated through an algebraic model. Before introducing this model, it is important to note that $V'(\Omega_e)$ is a subspace, thus Equation (13) can be manipulated such that we obtain a nonlinear partial differential equation to hold at each point in the interior of an element. This is crucial for the computational formulation to be presented later. The following algebraic model is introduced without deeper comments on its connection with Green's operators [2, 3, 15, 17], that is,

$$\mathbf{u}'=-\tau_\mathrm{M}\mathbf{r}_\mathrm{M} \tag{14}$$

where τ_M is a parameter to be set. Besides that, the model neglects the influence of p' in $\mathbf{u}'$ and then a heuristic scaling of the continuity equation motivates us to approximate the pressure fine-scales component as

$$p'=-\tau_\mathrm{C}\mathbf{r}_\mathrm{C} \tag{15}$$

DOI: 10.1002/fld

with $\mathbf{r}_C$ representing the residual of the continuity equation and τ_C is also a parameter to be set later. Now the relations (14) and (15) are substituted into Equation (13). Considering that only linear elements are employed here, applying integration by parts to the viscous term related to the velocity fine-scales component ends up on two vanishing terms. One, considering an integral over the domain, vanishes as it involves the Laplacian of the weighting functions. The other, encompassing the boundary, is disregarded as the meshes cover the border by element faces where $\mathbf{u}'=0$. Thus, the resulting equation representing the finite element problem to be solved is given by

$$\left(\frac{\partial \mathbf{u}^h}{\partial t}, \mathbf{w}^h\right)_\Omega + ((\mathbf{u}^h - \tau_M r_M)\cdot\nabla\mathbf{u}^h, \mathbf{w}^h)_\Omega + (\boldsymbol{\sigma}(p^h, \mathbf{u}^h), \boldsymbol{\varepsilon}(\mathbf{w}^h))_\Omega$$
$$+(\nabla\cdot\mathbf{u}^h, q^h)_\Omega + (\tau_M r_M, \mathbf{u}^h\cdot\nabla\mathbf{w}^h + \nabla q^h)_\Omega + (\tau_C\nabla\cdot\mathbf{u}^h, \nabla\cdot\mathbf{w}^h)_\Omega$$
$$-(\tau_M r_M, \tau_M r_M\cdot\nabla\mathbf{w}^h)_\Omega = (\mathbf{f}, \mathbf{w}^h)_\Omega + (\mathbf{h}, \mathbf{w}^h)_{\Gamma_h} \tag{16}$$

The integral after the velocity divergence term, involving the momentum coarse-scale residual can be interpreted as a stabilization term similar to the ones present in the SUPG/PSPG formulations (for a recent review, see [28]). The integral involving the continuity coarse-scale residual is a term similar to the LSIC stabilization, introduced in [27] and used to control oscillations at high Reynolds numbers flows. This observation was first made in Calo [5]. The last integral has been rearranged and if we add it to the stabilization integral we arrive at

$$\left(\frac{\partial \mathbf{u}^h}{\partial t}, \mathbf{w}^h\right)_\Omega + ((\mathbf{u}^h - \tau_M r_M)\cdot\nabla\mathbf{u}^h, \mathbf{w}^h)_\Omega + (\boldsymbol{\sigma}(p^h, \mathbf{u}^h), \boldsymbol{\varepsilon}(\mathbf{w}^h))_\Omega + (\nabla\cdot\mathbf{u}^h, q^h)_\Omega$$
$$+(\tau_M r_M, (\mathbf{u}^h - \tau_M r_M)\cdot\nabla\mathbf{w}^h + \nabla q^h)_\Omega + (\tau_C\nabla\cdot\mathbf{u}^h, \nabla\cdot\mathbf{w}^h)_\Omega$$
$$= (\mathbf{f}, \mathbf{w}^h)_\Omega + (\mathbf{h}, \mathbf{w}^h)_{\Gamma_h} \tag{17}$$

A remarkable fact present in Equations (16) and (17) is the convective velocity given by $\mathbf{u}^* = \mathbf{u}^h + \mathbf{u}' = \mathbf{u}^h - \tau_M\mathbf{r}_M$. Substituting the relation for $\mathbf{u}^*$ in Equation (17) we arrive at

$$\left(\frac{\partial \mathbf{u}^h}{\partial t}, \mathbf{w}^h\right)_\Omega + (\mathbf{u}^*\cdot\nabla\mathbf{u}^h, \mathbf{w}^h)_\Omega + (\boldsymbol{\sigma}(p^h, \mathbf{u}^h), \boldsymbol{\varepsilon}(\mathbf{w}^h))_\Omega + (\nabla\cdot\mathbf{u}^h, q^h)_\Omega$$
$$+(\tau_M r_M, \mathbf{u}^*\cdot\nabla\mathbf{w}^h + \nabla q^h)_\Omega + (\tau_C\nabla\cdot\mathbf{u}^h, \nabla\cdot\mathbf{w}^h)_\Omega = (\mathbf{f}, \mathbf{w}^h)_\Omega + (\mathbf{h}, \mathbf{w}^h)_{\Gamma_h} \tag{18}$$

which comprises an important difference when compared with former applications of the VMS approach to turbulence. Those formulations introduce a consistency error [5]. Moreover, the convective velocity encoded above is believed to better reproduce the physical mechanisms of eddies generation. The similarity of Equation (18) to the one resulting from the SUPG/PSPG/LSIC stabilized formulation is noteworthy. Certainly it can accommodate algorithms, data structures and procedures used for solving the resulting nonlinear problems, which are successfully used in stabilized methods and are addressed in the following section. Please note that this modified velocity does not disrupt the method's consistency.

DOI: 10.1002/fld

Here, the parameters τ_M and τ_C are computed simply by the standard expressions of stabilized methods,

$$\tau_M = \left(\frac{4}{\Delta t^2} + \left(\frac{\|\mathbf{u}^h\|}{h_\#} \right)^2 + 9 \left(\frac{\nu}{h_\#^2} \right)^2 \right)^{-1/2}, \quad \tau_C = \frac{h_\#}{3} \|\mathbf{u}^h\| \tag{19}$$

where $h_\#$ is the element length computed as the cubic root of the element volume and Δt is the time step. The formulae in Equation (19) can be tracked back to the original ones of [15, 17] through a linearization around homogenous stretched mappings relating reference and actual elements. Note, however, that the definition above is only recommended for simple elements, as the case of the linear tetrahedra used in the numerical experiments. For other elements, please use the general definitions in [15, 17].

3. SOLUTION PROCEDURE

The RB-VMS formulation presented in this work was implemented in the EdgeCFD software [13, 23], which is an incompressible flow solver able to treat free-surface flow problems by a VOF approach and density-driven flow. The finite element method in EdgeCFD is the SUPG/PSPG formulation plus LSIC stabilization for the incompressible Navier–Stokes equation and the SUPG formulation with discontinuity-capturing for scalar transport. Turbulence in EdgeCFD has been treated by a Smagorinsky model [23]. EdgeCFD is a parallel Fortran90 finite element code consisting of an outer time integration loop of two staggered-coupled systems of equations. Most of the computational cost comes from the $\mathbf{u}$–p coupled solution of the incompressible flow equations, while the cheapest part is due to the transport equation. Time integration is a predictor-multicorrector algorithm with adaptive time stepping by a proportional-integral-derivative controller (further details available in [31]). Within the flow solution loop, the multi-correction steps correspond to the inexact Newton method as described in [32]. In this method the tolerance of the linear solver is adapted according to the evolution of the solution residua. EdgeCFD iterative driver is the generalized minimal residual method (GMRES), since the equation systems stemming from the incompressible flow and transport are non-symmetric. Furthermore, a nodal block-diagonal and diagonal preconditioner are used respectively for flow and transport. Most of the computational effort spent in the solution phase is devoted to matrix–vector products. In order to compute such operations more efficiently, we have used an edge-based data structure as detailed in [32]. According to Ribeiro and Coutinho [25], this data structure, when applied to problems as those described in this work, is able to reduce the indirect memory access, the memory requirements to hold the coefficients of the stiffness matrices while decreasing the number of floating point operations per second when compared with other traditional data structures such as element-by-element of compressed sparse row. The computations are performed in parallel using a distributed memory paradigm through the message passing interface library. The parallel partitions are generated by the Metis library [33] while the information regarding the edges of the computational grid is obtained from the EdgePack library as described in [34]. EdgePack also reorders nodes, edges and elements to improve data locality, exploiting efficiently the memory hierarchy of current processors. Integrals in EdgeCFD are computed using closed-form relations derived in volume coordinates or using a one-point (centroid) integration rule. Thus, all coefficients in the element matrices and residua are explicitly coded.

DOI: 10.1002/fld

Therefore, if we evaluate $\mathbf{u}^*$ and the stabilization parameters τ_M and τ_C using values of the previous multi-correction, in a linearization scheme similar to the iteration-update of Tezduyar and Osawa [35] and Tezduyar [36], the RB-VMS implementation in EdgeCFD becomes straightforward. Moreover, in doing this, the only code modification required is the evaluation of $\mathbf{r}_M$ at the tetrahedra integration points. This is indeed very simple for straight-sided linear tetrahedra, requiring a few extra floating point operations and no additional memory but a few temporary variables.

4. NUMERICAL EXAMPLES

In order to assess the main characteristics of the formulation previously presented and test its feasibility in the context of high-performance computing, two examples are analyzed. They were chosen to cover different flow regimes, from laminar to turbulence, and to deal with engineering applications as well.

Please note that the RB-VMS computations shown in the following qualify this formulation as an important tool to be used within the realm of simulation of real flows. That is especially due to the fact that it does not require any LES-type modeling and, thus, can be applied to any region of the domain, regardless of the flow regime.

All computations were carried out in an SGI Altix 450 with 32 cores Intel Itanium2 processors, with 1.6 MHz/6 MB L2 and 2 GB of memory per processor.

4.1. Vortex shedding around a circular cylinder at $Re = 100$

The classical problem of vortex shedding around a circular cylinder at the Reynolds number $Re = 100$ is considered as an example of the ability of the present formulation to solve laminar incompressible flow problems. The computational domain follows the dimensions described in [32] and the mesh is formed by 446 662 linear tetrahedra, 1 010 367 edges and 81 991 nodes. The Reynolds number is based on the diameter of the cylinder, free-stream velocity and viscosity of the fluid. The boundary conditions are set as follows: no-slip condition at cylinder surface, $u = 1$ at domain inlet, zero-normal velocity and zero-shear stress at the lateral boundaries, traction-free conditions at the outflow boundary. Kalro and Tezduyar [37] noted that instabilities associated with three-dimensional effects occur in the vicinity of $Re = 190$. Figure 1 shows the cylinder surface mesh (a) and a vorticity snapshot (b), where well-defined von Karman vortex streets can be seen. These vortexes are almost uniform in the z-direction.

The simulation employed a fixed time step of 0.05 and 1000 time steps. The maximum inexact-Newton tolerance was set to 0.1 and the nonlinear loops were stopped after the relative residual or relative step increment decreased 3 orders of magnitude. The number of Krylov vectors for the preconditioned GMRES solver is set to 45. We compare in Figure 2 drag and lift coefficients for the present RB-VMS formulation with those computed, respectively, by SUPG/PSPG and SUPG/PSPG/LSIC. Note that the RB-VMS and the SUPG/PSPG/LSIC are in excellent agreement.

Another global variable of interest is the Strouhal number, defined as

$$St = \frac{D}{U_0}\omega \tag{20}$$

DOI: 10.1002/fld

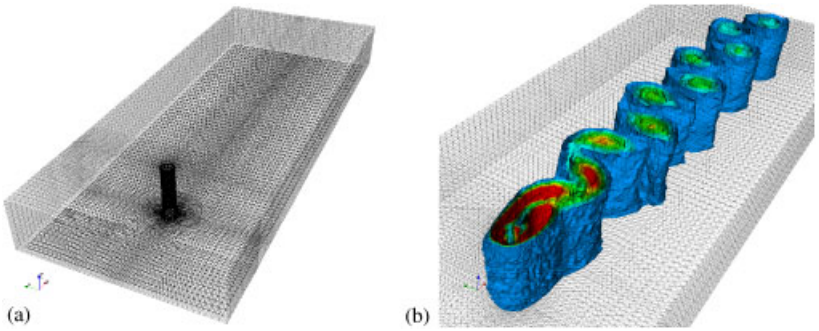

Figure 1. Flow around a circular cylinder at $Re = 100$: (a) mesh and (b) vorticity snapshot.

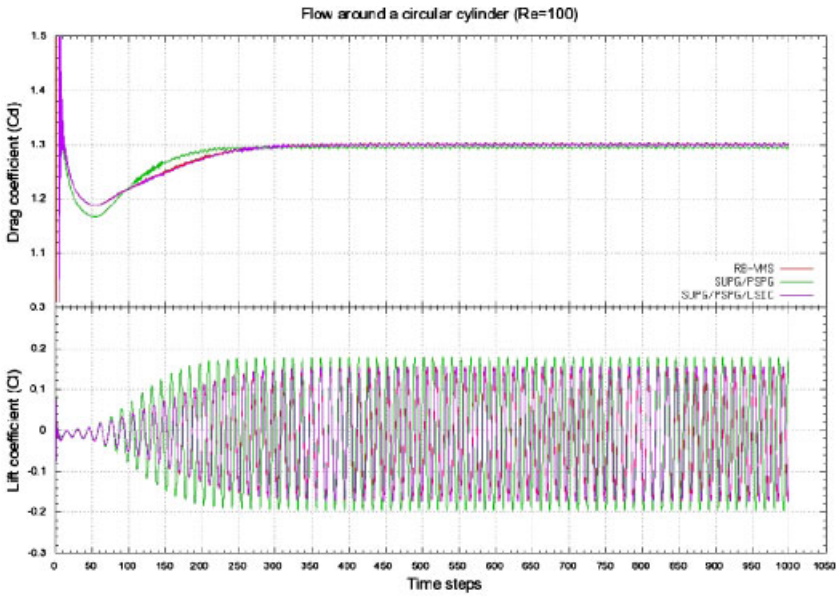

Figure 2. Drag and lift coefficients for the flow around a cylinder problem.

where D is the cylinder diameter, U_0 is the inflow velocity and ω is the vortex shedding frequency. The Strouhal number computed values for different formulations are given in Table I, where we also included a reference value computed numerically by Mittal [38] with a very fine mesh, with 933 180 nodes, around 10 times more than the present one. Mittal also used the SUPG/PSPG/LSIC formulation, but with trilinear hexahedra.

We can see that a good agreement is obtained for the Strouhal number. Figure 3 shows a qualitative comparison for velocity and pressure in two different time steps. In (a) we show the solutions at an early time step and in (b) solutions are in the periodic regimen. More pronounced differences can be seen for pressure at the early time step. The similarity between the RB-VMS and SUPG/PSPG solutions at this instant is however noteworthy.

DOI: 10.1002/fld

Table I. The Strouhal numbers for the circular cylinder.

FEM formulation	Strouhal number
RB-VMS	0.1523
SUPG/PSPG	0.1560
SUPG/PSPG/LSIC	0.1527
Mittal [38]	0.1610

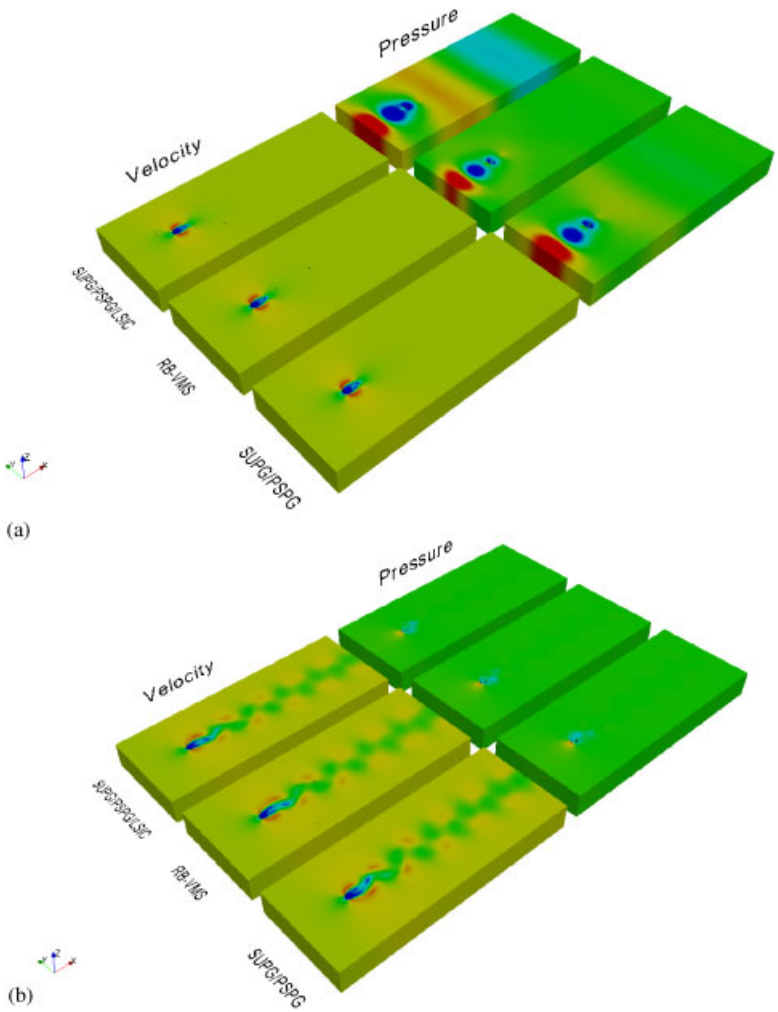

Figure 3. Velocity and pressure comparison for the circular cylinder problem: (a) velocity and pressure at $t = 0.003$ s and (b) velocity and pressure at $t = 0.272$ s.

DOI: 10.1002/fld

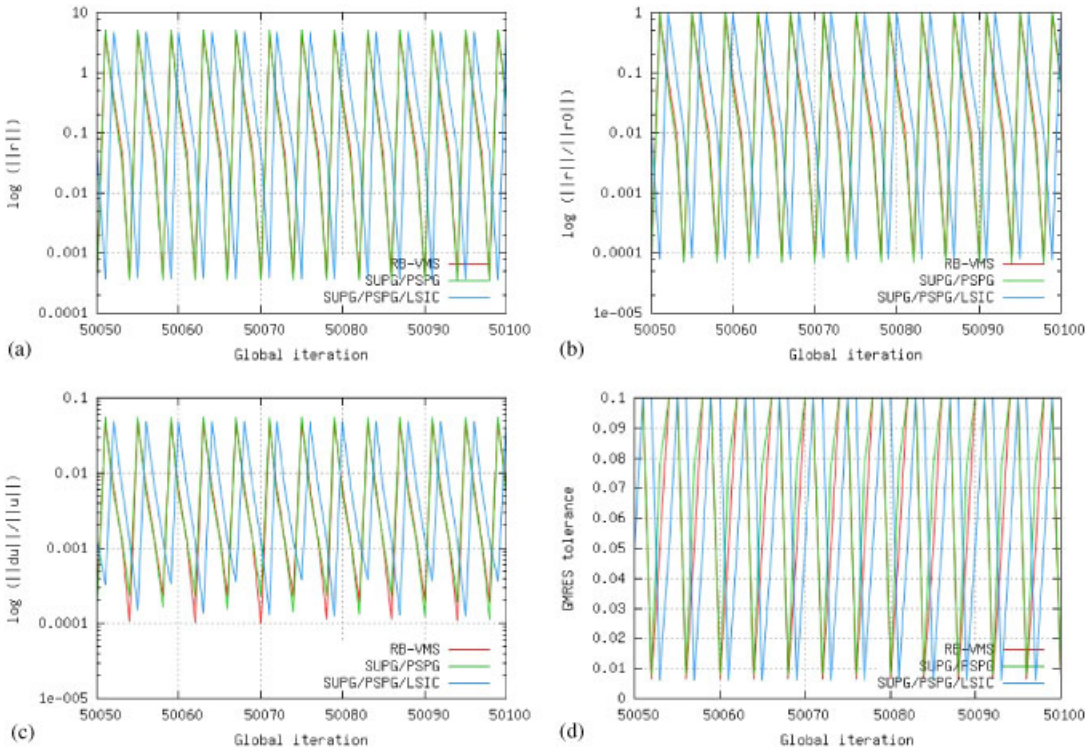

Figure 4. Performance analysis of inexact Newton method for the flow around a cylinder problem: (a) absolute residua; (b) relative residua; (c) relative solution increment; and (d) linear tolerance.

In Figure 4 we show a performance analysis of the inexact Newton method for RB-VMS, SUPG/PSPG and SUPG/PSPG/LSIC solutions. It is presented for a sequence of 50 time steps around $t = 625$ s, where the flow is already periodic, the evolution of the absolute residual (a), the relative residual (b), the solution increment (c) and the GMRES tolerance (d) for the inexact Newton iterations in this interval. The horizontal axis represents the global nonlinear iteration counter. We may note in Figure 4 that RB-VMS presents a performance equivalent to the SUPG/PSPG and SUPG/PSPG/LSIC solutions. In all time intervals we have observed a similar pattern. In the transition to the periodic regime, however, differences are more pronounced, with RB-VMS close to the SUPG/PSPG/LSIC solution.

4.2. Lid-driven cavity flow at $Re = 12\,000$

In the next test, the lid-driven cavity flow was solved for $Re = 12\,000$. This is a classic benchmark problem already addressed by a number of researchers (for a review of this problem, see [39]). Despite the simplicity of its geometry and boundary conditions, complex flow patterns are generated in this problem, especially at high Reynolds numbers. An SUPG/PSPG/LSIC computation, with the Smagorinsky model implemented as described in [23], was also used for comparison purposes. The Smagorinsky constant is fixed to be $C_S = 0.1$ and the length scale is taken as the cubic root of the element volume.

DOI: 10.1002/fld

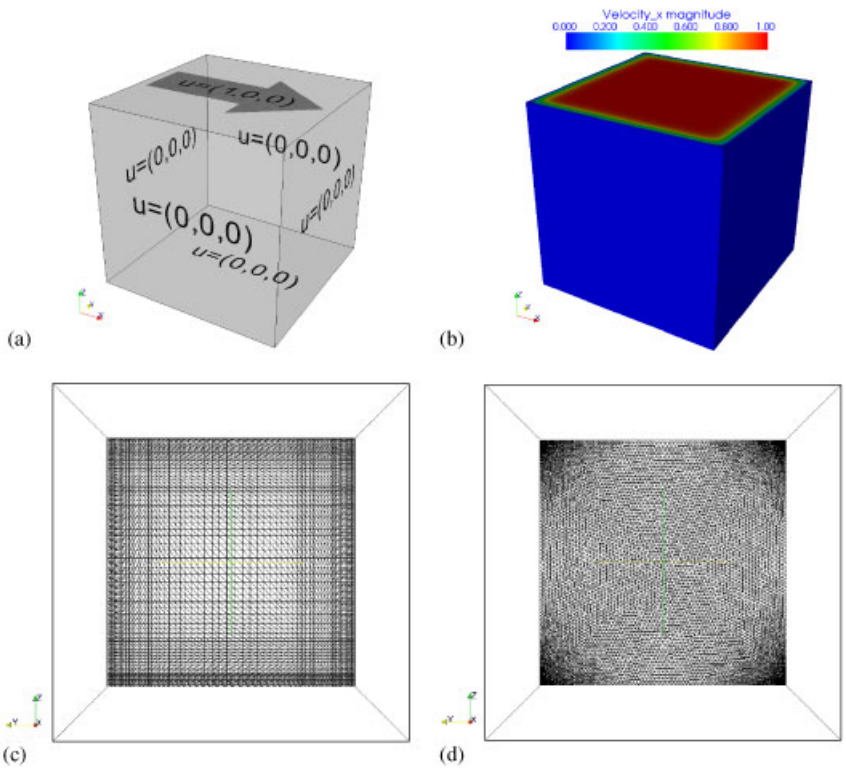

Figure 5. (a) Geometry, mesh and boundary conditions for lid-driven cavity flow; (b) velocity profile in the lid; (c) coarse; and (d) fine mesh at the cavity back wall.

The geometry and boundary conditions are shown in Figure 5(a). It consists of a cubical cavity with length L. The axis origin is at the center of cavity. To avoid discontinuities in Dirichlet boundary conditions, an approach similar to the one applied by Bouffanais *et al.* [29] is used to set the velocity profile in the lid:

$$u = U_0 \left(1 - \left(\frac{2x}{L}\right)^{18}\right)^2 \left(1 - \left(\frac{2y}{L}\right)^{18}\right)^2, \quad v = 0, \quad w = 0 \tag{21}$$

where u, v and w are the flow velocities at directions x, y and z, respectively. U_0 is the velocity in direction x at the lid. This velocity profile is shown in Figure 5(b). No-slip boundary conditions are set in all other walls. The Reynolds number is computed as $Re = LU_0/\nu$.

Aiming at analyzing the role of refining the spatial grids, two different meshes were employed. Both are regular at walls with respectively 64 and 128 element divisions at the edges, but distorted to improve mesh quality inside the domain. Figures 5(c) and (d) show the element distribution at the cavity back wall. The coarse mesh is formed by 643 070 linear tetrahedra elements, 117 196 nodes and 792 396 edges, while the fine mesh has 2 650 520 linear tetrahedra elements, 462 689 nodes and 3 159 654 edges.

DOI: 10.1002/fld

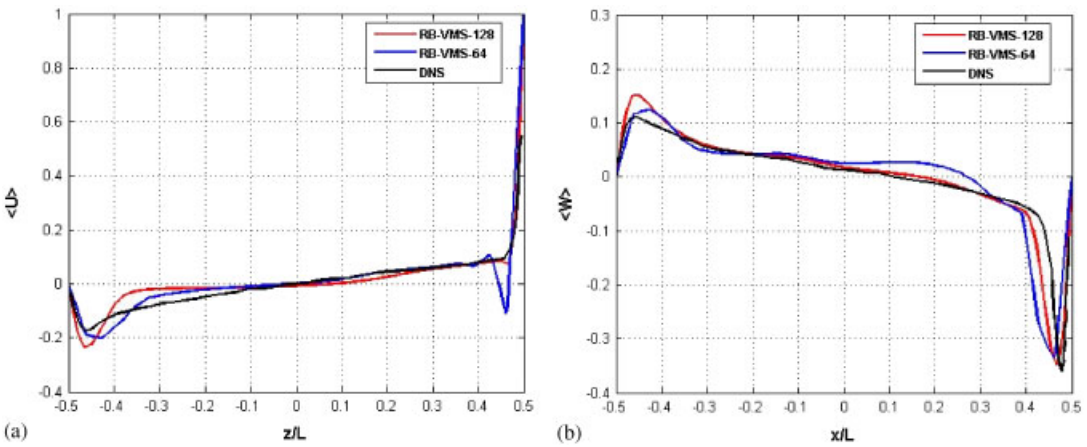

Figure 6. Velocity profiles in the mid-plane $y/L=0$ for different refining levels: (a) mean value of velocity in the x-direction and (b) mean value of velocity in the z-direction.

Table II. Numerical errors computed in mid-plane $y/L=0$.

$\langle U\rangle$ in z/L		$\langle W\rangle$ in x/L	
$e_{RB\text{-}VMS\text{-}64}$	0.2520	$e_{RB\text{-}VMS\text{-}64}$	0.4465
$e_{RB\text{-}VMS\text{-}128}$	0.2435	$e_{RB\text{-}VMS\text{-}128}$	0.2653

The simulations employed a fixed time step of 0.1 and 20 000 time steps (2000 time units). The maximum inexact Newton tolerance was set to 0.1 and the nonlinear loops were stopped after the relative residual or relative step increment decreased 3 orders of magnitude. We also limited to 7 the maximum number of inexact Newton iterations per time step. The number of Krylov vectors for the preconditioned GMRES solver is set to 200. The mean velocity at the cavity is calculated by time averaging each velocity component.

Although a detailed convergence analysis is not within the goals of this paper, the improvement through refining the mesh can be directly assessed by observing Figure 6. The velocity profiles in the mid-plane $y/L=0$ obtained with the RB-VMS formulation are compared with the DNS solution of Bouffanais *et al.* [29]. The improvement achieved through mesh refinement can be quantified by computing the error as the difference between the finite element results and some reference. In the present case the DNS was chosen, given rise to an average measure

$$e=\left(\frac{1}{N}\sum_{1}^{N}(u_{\mathrm{FEM}}-u_{\mathrm{DNS}})^2\right)^{1/2} \tag{22}$$

where N stands for the number of points. The obtained errors along different directions are summarized in Table II, where e has been computed along the symmetry plane.

Figure 7 shows the velocity profile at the cavity symmetry plane ($y/L=0$). Results are compared with the DNS and LES with a Dynamic Smagorinsky model solutions obtained by Bouffanais *et al.* [29], which used a spectral element method and the experimental measurements from

DOI: 10.1002/fld

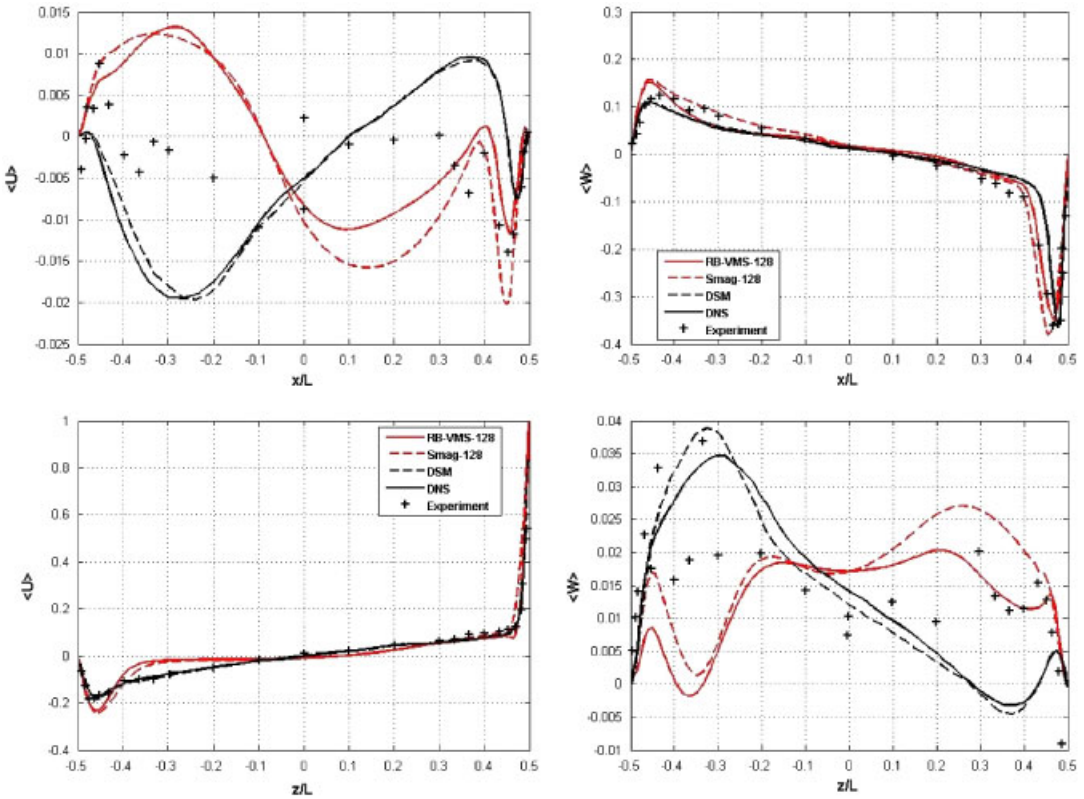

Figure 7. Velocity profiles in mid-plane $y/L=0$. Left side: mean value of velocity in the x-direction and right side: mean value of velocity in the z-direction.

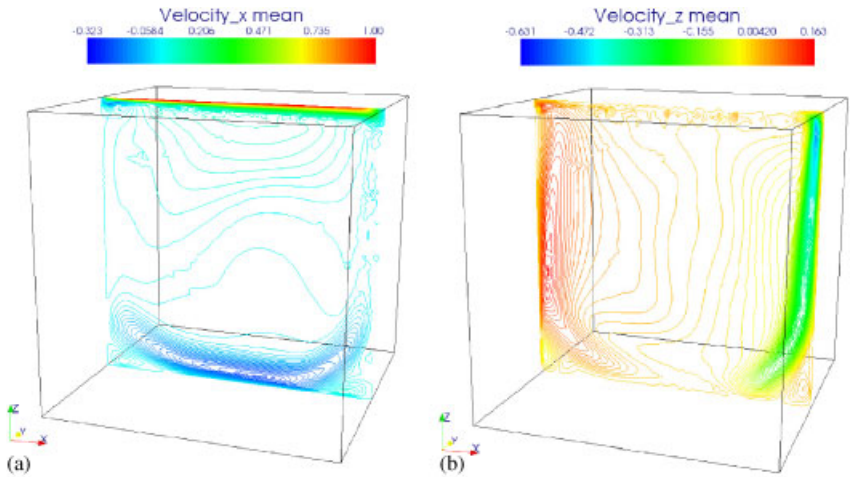

Figure 8. Contours of mean velocity in the cavity: (a) the x-component and (b) the z-component.

DOI: 10.1002/fld

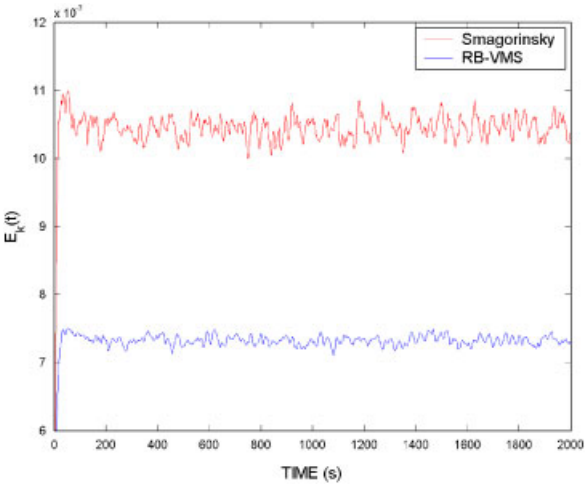

Figure 9. Time history of lid-driven cavity total kinetic energy.

Prasad and Koseff [40]. In Figure 7 and in subsequent figures the SUPG/PSPG/LSIC solution with the Smagorinsky model is identified simply as Smagorinsky. The improvement of the numerical results when refined grids are adopted is worth noting. The velocity obtained with the finer mesh gets closer to both the DNS and the experimental ones. Note though that an even finer mesh could improve these results.

In Figure 8 the mean velocity contours in the cavity mid-plane are presented. As can be observed, the main structures of flow (vortex position, velocity overall distribution) are present and the velocity ranges compares fairly well with the results in Bouffanais *et al*. [29]. Figure 9 shows the total kinetic energy temporal evolution given by

$$E_k(\mathbf{u}^h, t) = \frac{1}{2}\int_\Omega \mathbf{u}^h(t)\cdot\mathbf{u}^h(t)\,\mathrm{d}\Omega \tag{23}$$

We may observe that the total energy for the solution computed with the SUPG/PSPG/LSIC plus the Smagorinsky model is larger than using the RB-VMS formulation. This could be explained by noting that as the Smagorinsky model introduces viscosity through all scales of the resolved flow, a larger boundary layer around the lid tends to be formed, which ends up in more energy being transmitted to the cavity flow. This fact was already noted by Gravemeier *et al*. [41]. As long as the energy dissipation rate of this model is also elevated, high fluctuation of total energy can be expected. The RB-VMS, on the other hand, introduces much less numerical viscosity, and consequently the energy values and fluctuations induced by this model are comparatively smaller.

In order to further investigate the RB-VMS formulation, the local response at a point placed in a region of intense turbulence activity, located near the bottom of the cavity, was observed. This point, labeled as θ, was chosen quite close to the one pointed by Bouffanais *et al*. [29] as the site of maximum turbulence production. Its coordinates are given as $x/L=0.3956$; $y/L=0.1724$; $z/L=-0.4709$. Figure 10 depicts the total kinetic energy time history using both SUPG/PSPG/LSIC plus the Smagorinsky model and RB-VMS for point θ.

DOI: 10.1002/fld

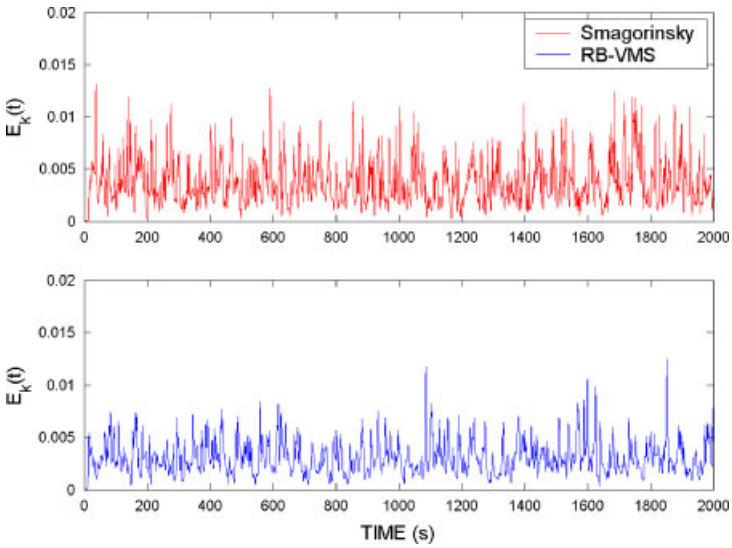

Figure 10. Time history of total kinetic energy at point θ.

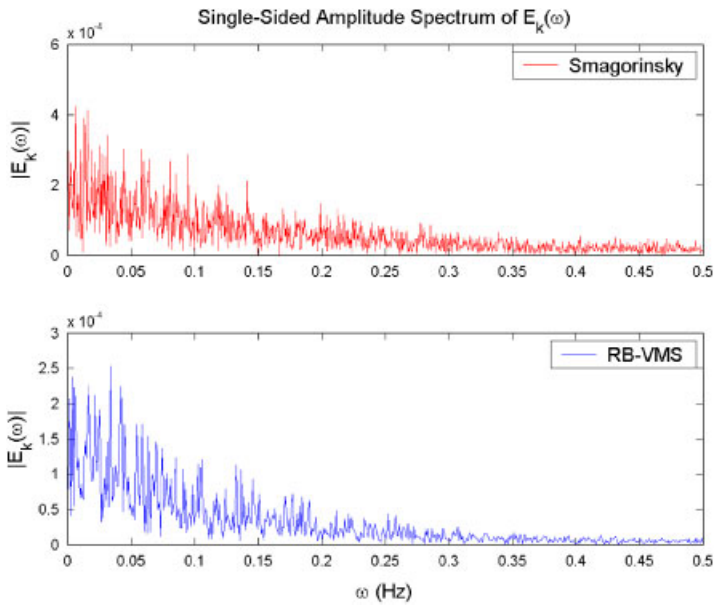

Figure 11. Fourier transform of total kinetic energy at point θ.

Turbulence reveals itself as a multiscale phenomenon also by the way energy is dissipated through a transfer among different scales, generating the so-called 'energy cascade'. This transfer mechanism can be better observed by transforming the time signals into its Fourier representation, as depicted in Figure 11, where the frequency ω gives the repetition period in the cavity flow.

DOI: 10.1002/fld

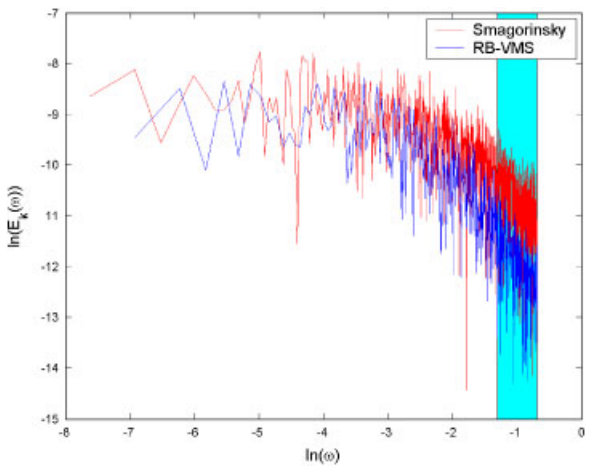

Figure 12. $\ln(\omega)\times\ln(|E_k(\omega)|)$ plot of Fourier transform of total kinetic energy at point θ.

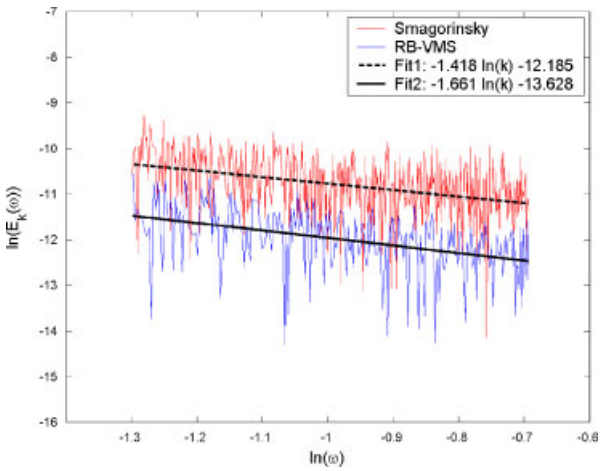

Figure 13. Line fit of Fourier transform of total kinetic energy at point θ in range $-1.3<\ln(\omega)<0$.

This Fourier transform can be used to evaluate the kinetic energy distribution according to the sizes of eddies. To this end, we consider the $\ln(\omega)\times\ln(|E_k(\omega)|)$ plot in Figure 12. In the range $-1.3<\ln(\omega)<0$, the data shown could be approximated by a linear relationship that could be expressed as $\ln(\omega)\approx C_0\ln(|E_k(\omega)|)$, where C_0 is a negative real constant. This plot has a resemblance with the Kolmogorov energy cascade and we note clearly the scale separation and the inertial subrange. A close inspection in the inertial subrange may provide a better insight into the behavior of RB-VMS. To this end, data for RB-VMS and SUPG/PSPG/LSIC plus the Smagorinsky model solutions in the highlighted region were selected for a linear fit.

This result is shown in Figure 13. The Kolmogorov theory states that in the inertial subrange, which is assumed to be partially covered by the employed space discretization, $E_k(\omega)\propto\omega^{-5/3}$.

DOI: 10.1002/fld

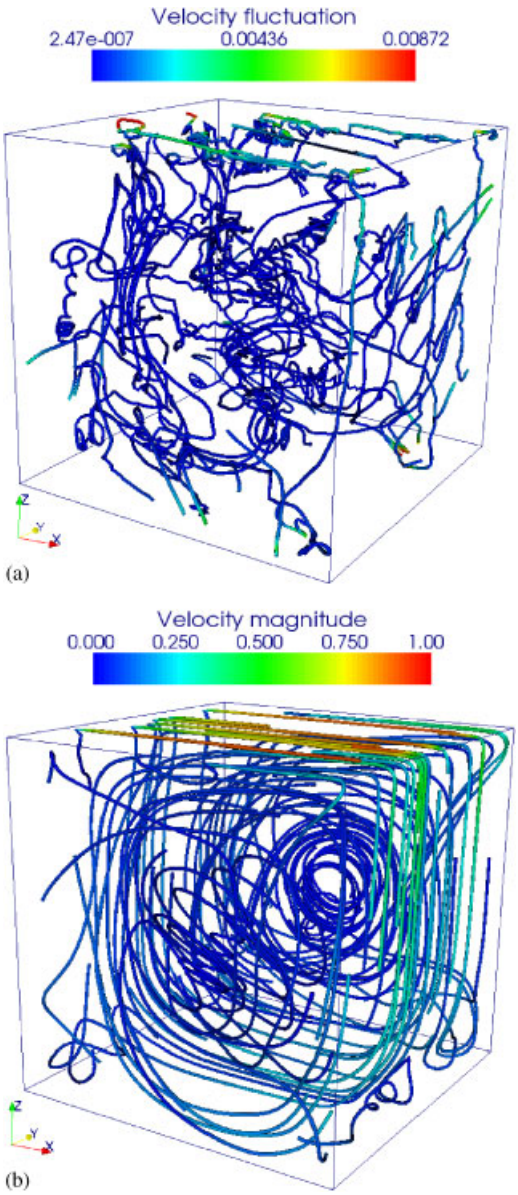

Figure 14. Mean fluctuation velocity (a) and mean velocity streamtubes (b).

As can be seen, the linear fit for the RB-VMS solution has a slope very close to $-\frac{5}{3}$, indicating that RB-VMS is able to represent this behavior much better than the stabilized formulation with the Smagorinsky model.

Figure 14 shows the computed mean fluctuation velocity ($\mathbf{u}'$) and mean velocity ($\mathbf{u}^h$) streamtubes for the RB-VMS solution. The streamtubes are colored based on the magnitudes and the presence

DOI: 10.1002/fld

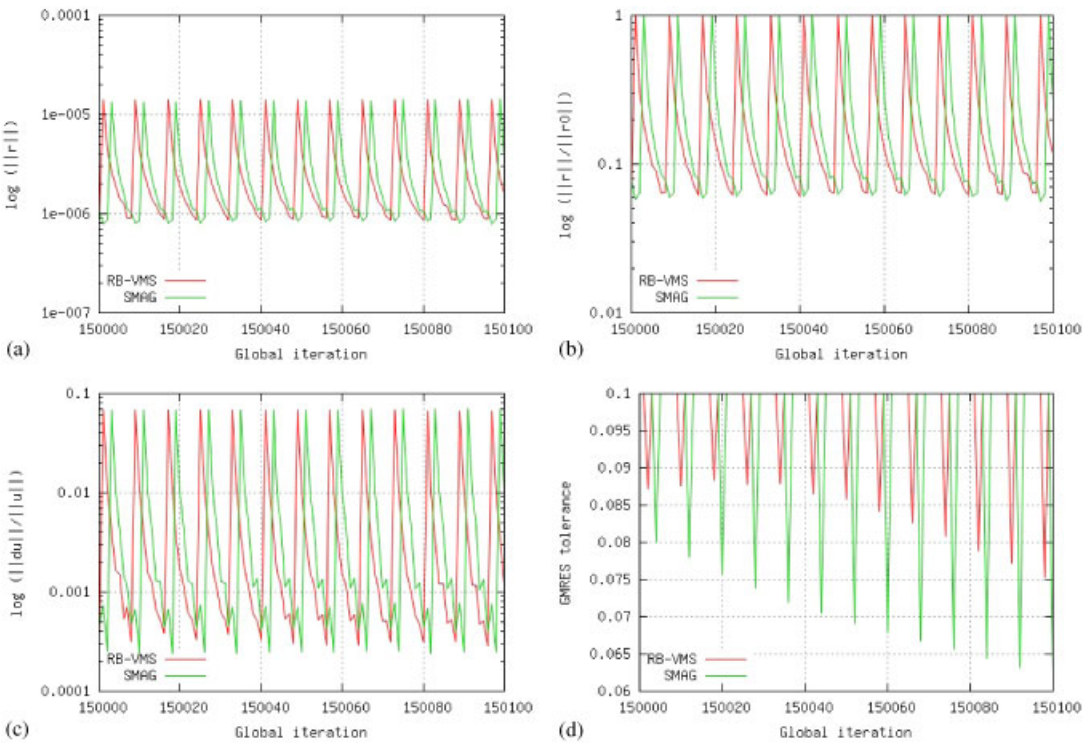

Figure 15. Performance analysis of inexact Newton method for the lid-driven cavity flow at $Re = 12\,000$: (a) absolute residua; (b) relative residua; (c) relative solution increment; and (d) linear tolerance.

of the main vortex, the secondary vortex near the bottom corner and many other vortical structures, typical from turbulent flow can be noted. In the mean fluctuation velocity plot, it is observed that magnitudes follow the velocity field. That is, it is higher in regions where the flow energy transfer is high.

In Figure 15 we show a performance analysis of the inexact Newton method for RB-VMS and our SUPG/PSPG/LSIC plus the Smagorinsky model solutions. We can see, for 15 time steps around $t = 1600$ s, the evolution of the absolute residual (a), the relative residual (b), the solution increment (c) and the GMRES tolerance (d) for the inexact Newton iterations in this interval. The horizontal axis represents the global nonlinear iteration counter. We observe in Figure 15 that RB-VMS presents a performance similar to the SUPG/PSPG/LSIC plus the Smagorinsky model solution. In this time interval, however, the computed GMRES tolerances for the inexact Newton method in RB-VMS are greater. In all other time intervals we have observed that performances are comparable.

5. CONCLUSIONS

In this work we have shown how to implement the residual-based variational multiscale (RB-VMS) method, using the advective-form of the convection term of the Navier–Stokes equations,

DOI: 10.1002/fld

as a straightforward extension of standard stabilized methods with a modified advective velocity. This requires minimum modification of the existing highly optimized finite element edge-based code for the incompressible Navier–Stokes equations with streamline-upwind/Petrov–Galerkin and pressure-stabilizing/Petrov–Galerkin (SUPG/PSPG) formulations plus the least-squares incompressibility constraint (LSIC) stabilization. A laminar and a turbulent test case was solved. We have shown that RB-VMS presents accuracy and performance similar to SUPG/PSPG/LSIC in the incompressible flow past a circular cylinder at $Re = 100$. We then compared our results in the lid-driven cubic cavity at $Re = 12\,000$ problem, where turbulent effects are present. We noted that the present implementation is able to capture most of the relevant turbulent flow features with reasonable accuracy when compared with highly resolved numerical simulations and experimental data. We also have shown that the present RB-VMS implementation has a computational performance comparable with the SUPG/PSPG/LSIC formulation with a classical Smagorinsky model.

ACKNOWLEDGEMENTS

The authors would like to thank the financial support of PETROBRAS Research Center and MCT/CNPq, The Brazilian Council for Scientific Research. Computer resources were provided by the Center of Parallel Computing, COPPE/UFRJ. During the preparation of this manuscript F.A. Rochinha was a Visiting Professor at the Institute of Applied Mathematics, University of British Columbia, Canada.

REFERENCES

1. Sagaut P, Deck S, Terracol M. *Multiscale and Multiresolution Approaches in Turbulence*. Imperial College Press: London, 2006.
2. Hughes TJR. Multiscale phenomena: Green's functions, the Dirichlet-to-Neumann formulation, subgrid scale models, bubbles and the origins of stabilized method. *Computer Methods in Applied Mechanics and Engineering* 1995; **127**:387–401.
3. Hughes TJR, Feijoo GR, Mazzei L, Quincy J-B. The variational multiscale method—a paradigm for computational mechanics. *Computer Methods in Applied Mechanics and Engineering* 1998; **166**:3–24.
4. Hughes TJR, Scovazzi G, Franca LP. Multiscale and stabilized methods. In *Encyclopedia of Computational Mechanics*, Stein E, de Borst R, Hughes TJR (eds). Wiley: Chichester, 2004.
5. Calo VM. Residual-based multiscale turbulence modeling: finite volume simulations of bypass transition. *Ph.D. Thesis*, Stanford University, 2004.
6. Gravemeier V. The variational multiscale method for laminar and turbulent flow. *Archives of Computational Methods in Engineering* 2006; **13**(2):249–324.
7. Akin JE, Tezduyar TE, Ungor M, Mittal S. Stabilization parameters and Smagorinsky turbulence model. *Journal of Applied Mechanics* 2003; **70**:2–9.
8. Hoffman J, Johnson C. A new approach to computational turbulence modeling. *Computer Methods in Applied Mechanics and Engineering* 2006; **195**:2865–2880.
9. Rispoli F, Corsini A, Tezduyar TE. Finite element computation of turbulent flows with the discontinuity-capturing directional dissipation (dcdd). *Computers and Fluids* 2007; **36**:121–126.
10. Tejada-Martinez AE, Jansen KE. On the interaction between dynamic model dissipation and numerical dissipation due to streamline upwind/Petrov–Galerkin stabilization. *Computer Methods in Applied Mechanics and Engineering* 2005; **194**:1225–1248.
11. de Sampaio PAB, Hallak PH, Coutinho ALGA, Pfeil MS. A stabilized finite element procedure for turbulent fluid–structure interaction using adaptive time-space refinement. *International Journal for Numerical Methods in Fluids* 2004; **44**:673–693.
12. de Sampaio PAB, Junior MAG, Lapa CMF. A CFD approach to the atmospheric dispersion of radionuclides in the vicinity of NPPs. *Nuclear Engineering and Design* 2007; DOI: 10.1016/j.nucengdes.2007.05.009.
13. Elias RN, Paraizo PLB, Coutinho ALGA. Stabilized edge-based finite element computation of gravity currents in lock-exchange configurations. *International Journal for Numerical Methods in Fluids* 2008; **57**(9):1137–1152.

14. Guasch O, Codina R. A heuristic argument for the sole use of numerical stabilization with no physical LES modeling in the simulation of incompressible turbulent flows. 2007. Available at: http://www.rmee.upc.es/homes/codina/guasch-codina-02.pdf.
15. Bazilevs Y, Calo VM, Cottrell JA, Hughes TJR, Reali A, Scovazzi G. Variational multiscale residual-based turbulence modeling for large eddy simulation of incompressible flows. *Computer Methods in Applied Mechanics and Engineering* 2007; **197**:173–201.
16. Gravemeier V, Lenz S, Wall WA. Variational multiscale methods for incompressible flows. *International Journal of Computing Science and Mathematics* 2007; **1**:444–466.
17. Akkerman I, Bazilevs Y, Calo VM, Hughes TJR, Hulshoff S. The role of continuity in residual-based variational multiscale modeling of turbulence. *Computational Mechanics* 2008; **41**(3):371–378.
18. Lohner R. *Applied CFD Techniques*. Wiley: New York, 2001.
19. Ribeiro FLB, Galeão AC, Landau L. Edge-based finite element method for shallow-water equations. *International Journal for Numerical Methods in Fluids* 2001; **36**:659–685.
20. Catabriga L, Coutinho ALGA. Implicit SUPG solution of Euler equations using edge-based data structures. *Computer Methods in Applied Mechanics and Engineering* 2002; **32**:3477–3490.
21. Soto O, Lohner R, Cebral JR, Camelli F. A stabilized edge-based implicit incompressible flow formulation. *Computer Methods in Applied Mechanics and Engineering* 2004; **193**:2139–2154.
22. Kraft RA, Coutinho ALGA, de Sampaio PAB. Edge-based data structures for a symmetric stabilized finite element method for the incompressible Navier–Stokes equations with heat transfer. *International Journal for Numerical Methods in Fluids* 2007; **53**:1473–1494.
23. Elias RN, Coutinho ALGA. Stabilized edge-based finite element simulation of free-surface flows. *International Journal for Numerical Methods in Fluids* 2007; **54**:965–993.
24. Elias RN, Martins MAD, Coutinho ALGA. Parallel edge-based solution of viscoplastic flows with the SUPG/PSPG formulation. *Computational Mechanics* 2006; **38**:365–381.
25. Ribeiro FLB, Coutinho ALGA. Comparison between element, edge and compressed storage schemes for iterative solutions in finite element analyses. *International Journal for Numerical Methods in Engineering* 2005; **63**(4): 569–588.
26. Brooks AN, Hughes TJR. Streamline-upwind/Petrov–Galerkin formulations for convection dominated flows with particular emphasis on the incompressible Navier–Stokes equations. *Computer Methods in Applied Mechanics and Engineering* 1982; **32**:199–259.
27. Behr M, Franca LP, Tezduyar TE. Stabilized finite element methods for the velocity-pressure-stress formulation of incompressible flows. *Computer Methods in Applied Mechanics and Engineering* 1993; **104**:31–38.
28. Tezduyar TE, Sathe S. Modelling of fluid–structure interactions with the space–time finite elements: solution techniques. *International Journal for Numerical Methods in Fluids* 2007; **54**:855–900.
29. Bouffanais R, Deville MO, Leriche E. Large-eddy simulation of the flow in a lid-driven cubical cavity. *Physics of Fluids* 2007; **19**:055108.
30. Codina R, Principe J, Guasch O, Badia S. Time dependent subscales in the stabilized finite element approximation of incompressible flow problems. *Computer Methods in Applied Mechanics and Engineering* 2007; **196**: 2413–2430.
31. Valli AMP, Carey GF, Coutinho ALGA. Control strategies for timestep selection in FE simulation of incompressible flows and coupled reaction–convection–diffusion processes. *International Journal for Numerical Methods in Fluids* 2005; **47**:201–231.
32. Elias RN, Martins MAD, Coutinho ALGA. *Parallel Edge-based Inexact Newton Solution of Steady Incompressible 3D Navier–Stokes Equations*. Lecture Notes in Computer Science, vol. 3648. Springer: Berlin, 2005; 1237–1245.
33. Karypis G, Kumar V. Metis 4.0: unstructured graph partitioning and sparse matrix ordering system. *Technical Report*, University of Minnesota, Minneapolis, U.S.A., 1998.
34. Coutinho ALGA, Martins MAD, Sydenstricker RM, Elias RN. Performance comparison of data-reordering algorithms for sparse matrix–vector multiplication in edge-based unstructured grid computations. *International Journal for Numerical Methods in Engineering* 2006; **66**:431–460.
35. Tezduyar TE, Osawa Y. Finite element stabilization parameters computed from element matrices and vectors. *Computer Methods in Applied Mechanics and Engineering* 2000; **190**:411–430.
36. Tezduyar TE. Computation of moving boundaries and interfaces and stabilization parameters. *International Journal for Numerical Methods in Fluids* 2003; **43**:555–575.
37. Kalro V, Tezduyar T. Parallel 3D computation of unsteady flows around circular cylinders. *Parallel Computing* 1997; **23**:1235–1248.

DOI: 10.1002/fld

38. Mittal S. Computation of three-dimensional flows past circular cylinder of low aspect ratio. *Physics of Fluids* 2001; **13**(1):177–191.
39. Albensoeder S, Kuhlmann HC. Accurate three-dimensional lid driven cavity flow. *Journal of Computational Physics* 2005; **206**:536–558.
40. Prasad AK, Koseff JR. Reynolds number and end-wall effects on a lid-driven cavity flow. *Physics of Fluids A* 1989; **1**:208–218.
41. Gravemeier V, Wall WA, Ramm E. Large eddy simulation of turbulent incompressible flows by a three-level finite element method. *International Journal for Numerical Methods in Fluids* 2005; **48**:1067–1099.

DOI: 10.1002/fld